Proceedings Paper:
Yang, Y, Wang, Z and Yu, H-S (2014) A soil model considering principal stress rotations. In: Hicks, MA, Brinkgreve, RBJ and Rohe, A, (eds.) Numerical Methods in Geotechnical Engineering: Proceedings of the 8th European Conference on Numerical Methods in Geotechnical Engineering. NUMGE 2014: 8th European Conference on Numerical Methods in Geotechnical Engineering, 18-20 Jun 2014, Delft, The Netherlands. CRC Press, pp. 1319-1324. ISBN: 9781138001466.

A Soil Model Considering Principal Stress Rotations

Yunming Yang
Department of Civil Engineering, University of Nottingham Ningbo China, China
Zhe Wang
Department of Civil Engineering, University of Nottingham Ningbo China, China
Hai-Sui Yu
Nottingham Centre for Geomechanics, University of Nottingham, UK

ABSTRACT: This paper presents an elastoplastic soil model considering the principal stress rotation (PSR). The model is developed on the basis of a well-established kinematic hardening soil model using the bounding surface concept. The impact of the stress rate generating the PSR is treated independently, and is added to the base kinematic hardening model. The significance of independent treatment of the PSR stress rate in the soil model is demonstrated through comparing the simulations of soil stress-strain responses by using the base soil model and the modified model in the paper. Various test results in different sands under both drained and undrained conditions are simulated. The paper also discusses the simulations of sand responses under multiple PSRs.

1 INTRODUCTION

Many types of loadings in geotechnical engineering can generate the principal stress rotation (PSR) in soil, such as the earthquake, wave and traffic loading (Ishihara & Towhata, 1983; Ishihara, 1993; Grabe & Clayton, 2009). Numerous experimental studies indicate that a change of principal stress directions, without a change of principal stress magnitudes, can lead to plastic deformations in soil (Roscoe et al, 1967; Miura et al, 1986; Gutierrez et al, 1991; Chen & Kutter, 2009). Further, the principal strain increment directions are not coincident with the principal stress directions under the PSR, and this non-coincidence is called the non-coaxiality. Neglecting the PSR induced deformations can lead to unsafe designs, especially the volumetric strain, such as in the study of sand liquefaction. In conventional elastoplastic theory, the stress rate generating the PSR and the stress rate not associated with the PSR are treated the same way, so that the soil behavior can not be properly simulated under the loading including the PSR. A few elastoplastic constitutive models have been developed to treat the PSR stress rate and non-PSR stress rate separately in their model formulations (Gutierrez et al, 1991; Tsutsumi & Hashiguchi, 2005; Yang & Yu, 2006; Li & Dafalias, 2006). However, some of them can only properly simulate part of aspects involving the PSR, such as the non-coxiality. Some are complicated and not easy to be numerically implemented. This paper aims to develop a soil model which can properly represent all characteristics of soil responses induced by the PSR in a relatively concise way. For this purpose, a well-established kinematic hardening soil model with the bounding surface concept is used a base model (Dafalias & Manzari, 2004). Model simulations with and without the special treatment of PSR stress rate will be compared with test results. Since there are multiple PSRs along different directions in many occasions in geotechnical engineering, attempts are also made to study the impact of multiple PSRs.

2 THE ORIGINAL BASE MODEL

The total strain rate $d\boldsymbol{\varepsilon}$ can be broken down into the elastic $d\boldsymbol{\varepsilon}^e$ and plastic component $d\boldsymbol{\varepsilon}^p$, which is composed of $d\boldsymbol{\varepsilon}_m^p$ from the stress rate without the PSR $d\boldsymbol{\sigma}_m$, named as the monotonic loading for simplicity, and the $d\boldsymbol{\varepsilon}_r^p$ from the PSR $d\boldsymbol{\sigma}_r$, where the subscript *m* and *r* represent the monotonic loading and PSR loading hereafter, respectively. $d\boldsymbol{\varepsilon}^e$ and $d\boldsymbol{\varepsilon}_m^p$ can be obtained by the conventional elastoplasticity theory. A well-established soil model with the kinematic hardening and bounding surface concept is used (Dafalias & Manzari, 2004) as the base model, which doesn't consider the PSR. Its formulations are briefly presented in this section, and the details can be found in Dafalias & Manzari (2004). The yield function of model is,

$$f = [(\mathbf{s} - p\boldsymbol{\alpha}) : (\mathbf{s} - p\boldsymbol{\alpha})]^{1/2} - \sqrt{2/3}\, pm = 0 \qquad (1)$$

where ***s*** and *p* are deviatoric stress tensor and confining pressure, respectively. $\boldsymbol{\alpha}$ is the back-stress ratio

representing the center of yield surface, and m is the radius of yield surface on the deviatoric plane with a very small constant. $d\boldsymbol{\varepsilon}_m^p$ is given as,

$$d\boldsymbol{\varepsilon}_m^p = \langle L_m \rangle \mathbf{R}_m = \frac{1}{K_{pm}} \left(\frac{\partial f}{\partial \boldsymbol{\sigma}} d\boldsymbol{\sigma}_m\right) \mathbf{R}_m \quad (2)$$

where L_m represents the loading index, K_{pm} is the plastic modulus and R_m represents the flow direction. K_{pm} is defined as,

$$K_{pm} = \frac{2}{3} p \left[G_0 h_0 (1 - c_h e) \left(\frac{p}{p_{at}} \right)^{-1/2} \right] \left[\frac{|\mathbf{b} : \mathbf{n}|}{|(\boldsymbol{\alpha} - \boldsymbol{\alpha}_{in}) : \mathbf{n}|} \right] \quad (3)$$

where $\mathbf{b}$ is the distance between the current back-stress ratio tensor and bounding back-stress ratio tensor on the bounding surface. G_0, h_0 and c_h are the plastic modulus model parameters. $\mathbf{R_m}$ is defined as,

$$\mathbf{R_m} = \mathbf{n} + \frac{1}{3} D_m \mathbf{I} = \mathbf{n} + \frac{1}{3} A_d (\mathbf{d} : \mathbf{n}) \mathbf{I} \quad (4)$$

where $\mathbf{n}$ represents the normal to the yield surface on the deviatoric plane, and D_m is the dilatancy ratio. $\mathbf{d}$ is the distance between the current back-stress ratio tensor and dilatancy back-stress ratio tensor, and A_d is a dilatancy model parameter.

The model is first used to predict stress-strain responses of Toyoura sand under drained conditions, in which several typical stress paths are studied. One is the monotonic loading paths (F paths) in which monotonic loadings are applied at different angles with the horizontal bedding plane (Miura et al, 1986). This is also used to calibrate model parameters. Another loading path is the pure PSR path (R paths), in which the stress ratio $(\sigma_a - \sigma_t)/(\sigma_a + \sigma_t)$ is chosen to be 0.5 (R1) and 0.6 (R2), respectively (Miura et al, 1986). The third loading tests are performed by Gutierrez et al (1991), in which the non-coaxiality is measured at different mobilized frictional angles. In all those tests, the confining pressure remains constant at 98 kPa, and b remains constant at 0.5. Figure 1 shows the tests results and model predictions for the monotonic tests, and a reasonably good agreement is achieved. It is noted that this model doesn't consider the role of fabric anisotropy, and its simulations are intended to fit the average of all tests results along different loading directions. Table 1 shows the model parameters calibrated in the monotonic loading test.

Figure 2 shows the evolutions of various strain components including the volumetric strain with rotational angles of principal stress in tests results and predictions for the PSR path R1. Figure 3 shows the tests results and predictions for the PSR path R2, starting at $2\alpha = 180^0$. Figure 2 shows a reasonably good agreement between the test results and predictions in the PSR path R1, except for the radial strain, which is much smaller than other strain components and can be neglected. However, Figure 3 shows the discrepancy between the predicted and measured results is much larger in R2 than in R1, especially for the shear strain and volumetric strain. The predicted volumetric strain is much smaller than that measured in the test.

Table 1. Model parameters in the original and modified models for Toyoura sand (the first line) and Nevada sand (the second line)

original model							
elasticity		critical state					Y.S.
G_0	ν	M	c	λ_c	e_0	ξ	m
125	0.25	1.25	0.712	0.019	0.934	0.7	0.01
150	0.2	1.45	0.689	0.0052	0.807	0.5	0.01
plasticity			dilatancy		modified model		
h_0	c_h	n^b	A_0	n^d	h_{0r}	ξ^r	A_r
15	0.968	1.1	0.8	0.9	10	1.5	0.4
5.5	0.968	0.55	0.6	3.5	0.9	1.1	0.18

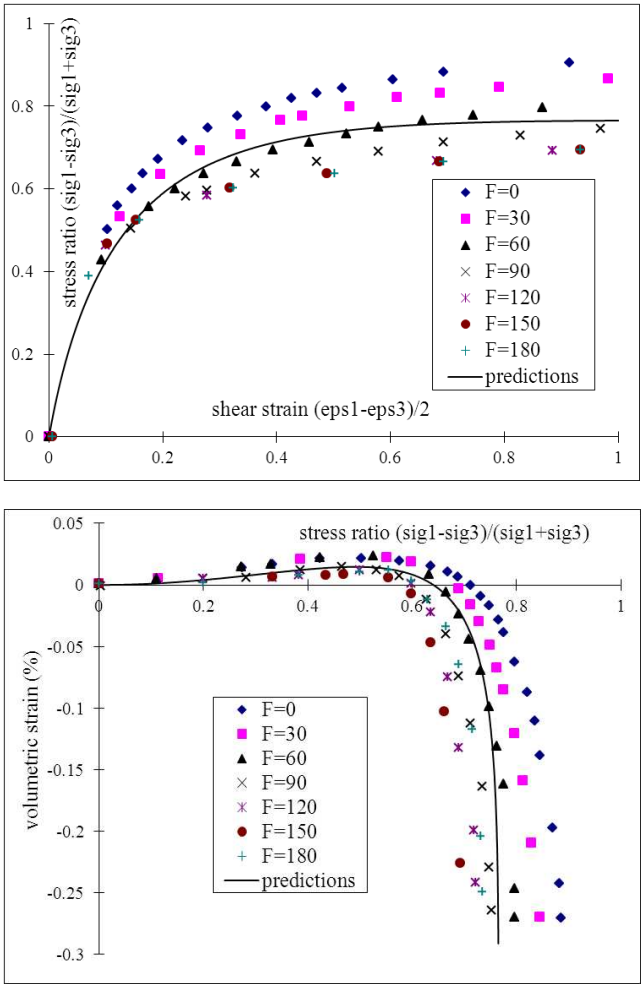

Figure 1. Test results and model predictions of the monotonic loadings in Miura et al (1986) for Toyoura sand (F denotes the angle of loading).

It is because the stress ratio in R2 is close to dilatancy surface or the phase transformation line, which results in a smaller predicted volumetric contraction. If the PSR occurs at a stress ratio a little higher than that in R2 or above the phase transformation line ($(\sigma_a - \sigma_t)/(\sigma_a + \sigma_t) = 0.65$), the volumetric expansion is even generated in simulations, which is shown in Figure 3. The poor prediction of volumetric strain has a serious consequence in the study of undrained soil behaviors in which the plastic volumetric strain

directly controls the generation of pore water pressures. The discrepancy is understandable as the model doesn't distinguish the PSR and non-PSR stress rate, and all the model parameters are calibrated in the monotonic loadings. Figure 4 shows the predicted and measured non-coaxiality at various mobilized friction angles, and they are in a very good agreement. The larger the mobilized friction angle is, the smaller the non-coaxiality becomes. This is because, according to the projection rule of the bounding surface concept used in this model and many other kinematic models, the direction of plastic flow on the deviatoric plane gets closer to that for the principal stresses at a higher stress ratio when it approaches the bounding surface.

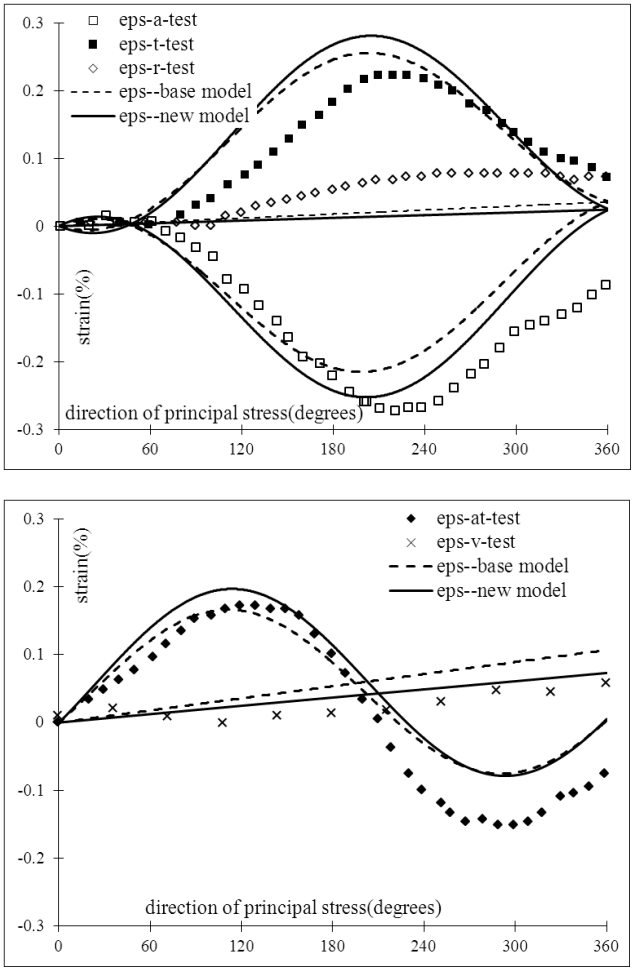

Figure 2. Test results and predictions of PSR loadings *R1* in Miura et al (1986) with the original base model and the modified new model (eps-a: axial strain; eps-t: circumferential strain; eps-r: radial strain; eps-at: shear strain; eps-v: volumetric strain).

The model is also used to reproduce stress-strain responses of Nevada sand with three stress paths in hollow cylinder tests. The first one is the drained triaxial compression with various initial confining pressures and relative densities. In the second path called the torsional shear, the soil specimen is first subjected to drained triaxial extension loading with K_0=1.38, followed by a cyclic loading of shear stress under undrained conditions until liquefaction occurs. Because the loading starts with the initial anisotropic condition and the effective confining pressure can't reach zero, and the liquefactions manifest themselves through large deformations. In the third path called the rotational shear, the soil is subjected to continuous principal stress rotations under undrained conditions. Figure 5 shows typical test results and simulations under triaxial compressions, and they are used to calibrate model parameters, shown in Table 1. Figure 6 and 7 show the test results and model simulations under the second and third stress paths. These two figures indicate that the model predictions are unable to bring the soil to liquefactions.

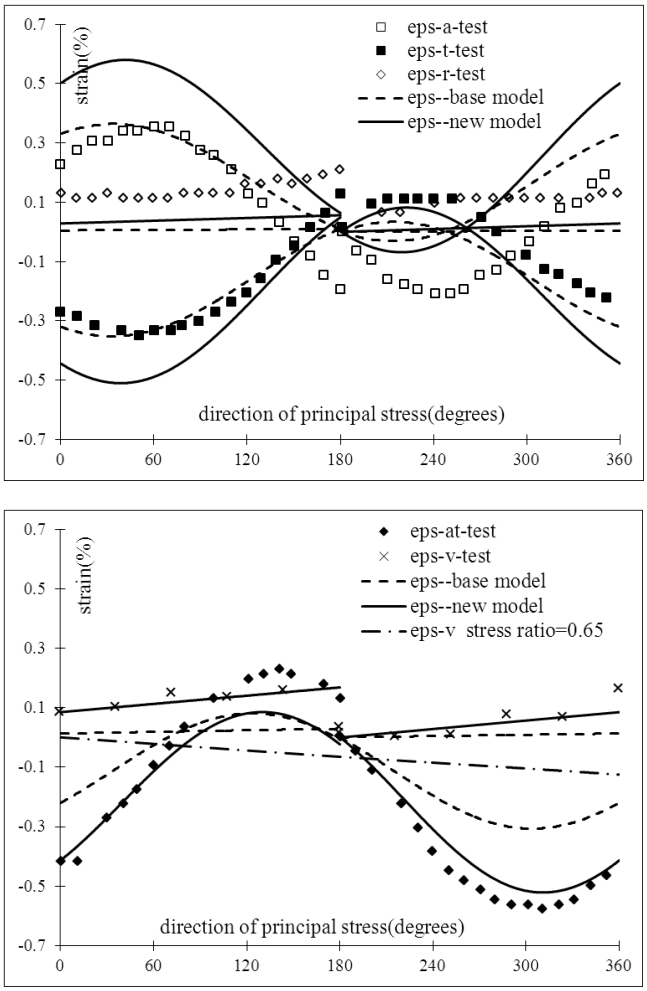

Figure 3. Test results and predictions of PSR loadings *R2* in Miura et al (1986) and the volumetric strain for the additional stress ratio (0.65) with the original base model and the modified new model

3 THE MODIFIED MODEL WITH THE PSR

In the modified model, the stress rate component generating the PSR is treated independently. One can refer to Yang & Yu (2012) for detailed descriptions, and a brief description is presented in this section. $d\boldsymbol{\varepsilon}_r^p$ generated from $d\boldsymbol{\sigma}_r$ is given as,

$$d\boldsymbol{\varepsilon}_r^p = \langle L_r \rangle \mathbf{R}_r = \frac{1}{K_{pr}} \left(\frac{\partial f}{\partial \boldsymbol{\sigma}} d\boldsymbol{\sigma}_r \right) \mathbf{R}_r \tag{5}$$

$$K_{pr} = \frac{2}{3} p \left[G_0 h_{0r} (1 - c_h e) \left(\frac{p}{p_{at}} \right)^{-1/2} \right] \left(\frac{|\mathbf{b} : \mathbf{n}|}{|(\boldsymbol{\alpha} - \boldsymbol{\alpha}_{in}) : \mathbf{n}|} \right)^{\xi_r} \quad (6)$$

where L_r is the loading index, K_{pr} plastic modulus and $\mathbf{R}_r$ flow direction from the PSR. h_{0r} and ξ_r are new model parameters for the PSR plastic modulus. The PSR plastic modulus is similar to that for the monotonic loading except the addition of ξ_r. ξ_r is generally larger than unity, which makes K_{pr} more sensitive to the stress ratio.

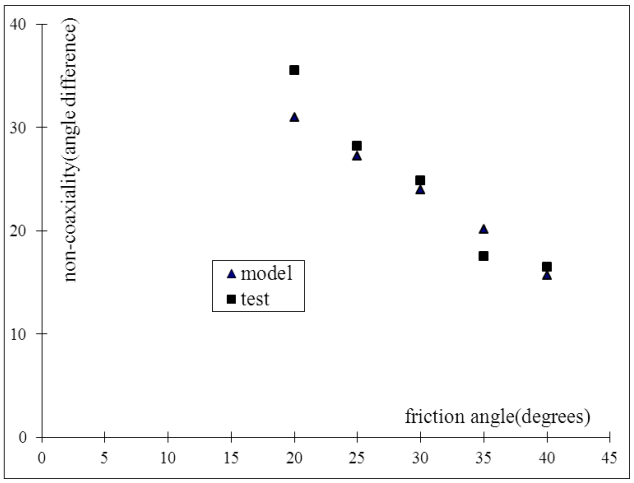

Figure 4. Measured and predicted non-coaxiality for the PSR loadings at various stress ratios in Gutierrez et al (1991)

$\mathbf{R}_r$ is defined as,

$$\mathbf{R}_r = \mathbf{n}_r + \frac{1}{3} D_r \mathbf{I} = \mathbf{n}_r + \frac{1}{3} A_r \left(\mathbf{1} - \frac{\alpha}{\alpha_\theta^b} \right) \mathbf{I} \quad (7)$$

where D_r is the dilatancy ratio, and A_r is the dilatancy model parameter for the PSR loading. α and α_θ^b are the amplitudes of back-stress ratio and bounding back-stress ratio. $\mathbf{n_r}$ can be approximated to be $\mathbf{n}$ in many cases. The determination of D_r uses the postulate for the PSR dilatancy rule by Gutierrez et al (1991). Thus, three new PSR related model parameters are used in the modified model. They are independent of the monotonic loading, and can be easily obtained through pure PSR loading paths at different stress ratio levels.

The final task is to determine $d\boldsymbol{\sigma}_r$. It is first determined in two dimension (x, y), denoted with α. It can be expressed as $d\boldsymbol{\sigma}_r^\alpha = \mathbf{N}_r^\alpha d\boldsymbol{\sigma}$, written in a matrix form as,

$$\begin{pmatrix} d\sigma_{rx}^\alpha \\ d\sigma_{ry}^\alpha \\ d\sigma_{rxy}^\alpha \end{pmatrix} = \begin{bmatrix} \frac{1}{2} - \frac{(\sigma_x - \sigma_y)^2}{8t_J^\alpha} & -\frac{1}{2} + \frac{(\sigma_x - \sigma_y)^2}{8t_J^\alpha} & -\frac{(\sigma_x - \sigma_y)\sigma_{xy}}{2t_J^\alpha} \\ -\frac{1}{2} + \frac{(\sigma_x - \sigma_y)^2}{8t_J^\alpha} & \frac{1}{2} - \frac{(\sigma_x - \sigma_y)^2}{8t_J^\alpha} & \frac{(\sigma_x - \sigma_y)\sigma_{xy}}{2t_J^\alpha} \\ -\frac{(\sigma_x - \sigma_y)\sigma_{xy}}{4t_J^\alpha} & \frac{(\sigma_x - \sigma_y)\sigma_{xy}}{4t_J^\alpha} & 1 - \frac{\sigma_{xy}^2}{t_J^\alpha} \end{bmatrix} \begin{pmatrix} d\sigma_x \\ d\sigma_y \\ d\sigma_{xy} \end{pmatrix} \quad (8)$$

where $t_J^\alpha = (\sigma_x - \sigma_y)^2 / 4 + \sigma_{xy}^2$. Similarly, in the space (y, z) denoted with β and (z, x) with γ, they can be expressed as $d\boldsymbol{\sigma}_r^\beta = \mathbf{N}_r^\beta d\boldsymbol{\sigma}$ and $d\boldsymbol{\sigma}_r^\gamma = \mathbf{N}_r^\gamma d\boldsymbol{\sigma}$. Combining $d\boldsymbol{\sigma}_r^\alpha$, $d\boldsymbol{\sigma}_r^\beta$ and $d\boldsymbol{\sigma}_r^\gamma$, letting $d\sigma_{rx} = d\sigma_{rx}^\alpha + d\sigma_{rx}^\gamma$, $d\sigma_{ry} = d\sigma_{ry}^\alpha + d\sigma_{ry}^\beta$ and $d\sigma_{rz} = d\sigma_{rz}^\beta + d\sigma_{rz}^\gamma$, one can obtain $d\boldsymbol{\sigma}_r$ in the general stress space,

$$d\boldsymbol{\sigma}_r = \mathbf{N}_r d\boldsymbol{\sigma} \quad (9)$$

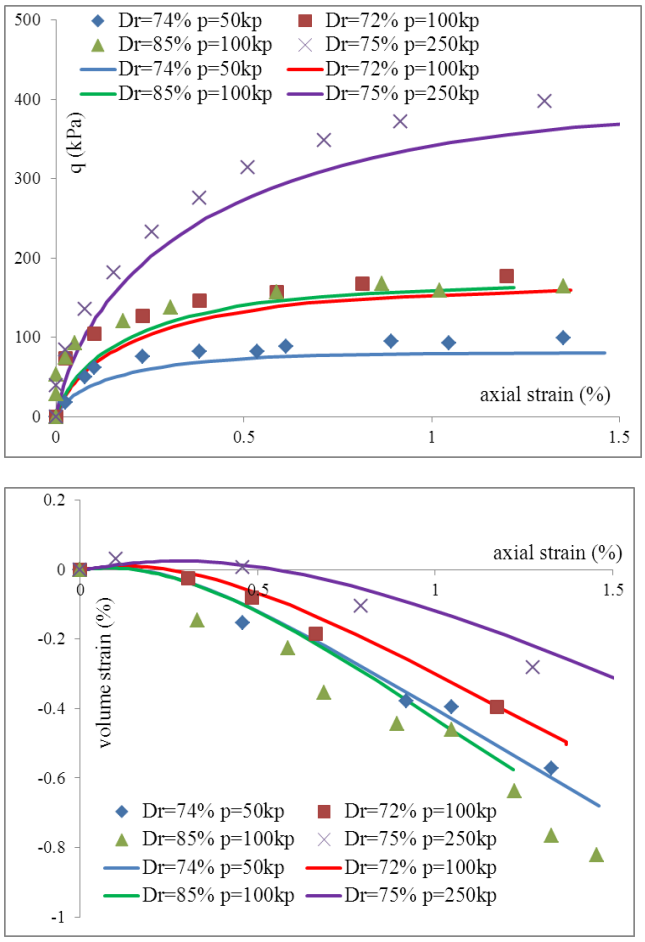

Figure 5. Test results and model predictions of the monotonic loadings in Chen & Kutter (2009) for Nevada sand

The total stress increment can be expressed as,

$$d\boldsymbol{\sigma} = \mathbf{E}(d\boldsymbol{\varepsilon} - d\boldsymbol{\varepsilon}^p) = \mathbf{E}(d\boldsymbol{\varepsilon} - d\boldsymbol{\varepsilon}_m^p - d\boldsymbol{\varepsilon}_r^p) \quad (10)$$

where $\mathbf{E}$ represents the elastic stiffness tensor. Using mathematical manipulations and the relationship

$$\mathbf{E}\mathbf{N}_r = 2G\mathbf{N}_r \quad (11)$$

One can obtain,

$$d\boldsymbol{\sigma} = \mathbf{E}^{ep} d\boldsymbol{\varepsilon} \quad (12)$$

$$\mathbf{E}^{ep} = \mathbf{E} - B_1 \left[\frac{(\mathbf{ER})(\mathbf{IN}_r^*)}{K_{pr} + \mathbf{IN}_r^* \mathbf{R}_r} - \frac{(\mathbf{ER})(\mathbf{IE})}{K_{pr} + \mathbf{IER}_r} \right] - B_2 \left[\frac{(\mathbf{ER}_r)(\mathbf{IN}_r^*)}{\mathbf{IN}_r^* \mathbf{R}} - \frac{(\mathbf{ER}_r)(\mathbf{IE})}{K_p + \mathbf{IER}} \right] \quad (13)$$

$$\mathbf{N}_r^* = 2G\mathbf{N}_r \quad (14)$$

$$B_1 = \left(\frac{\mathbf{IN}_r^* \mathbf{R}}{K_{pr} + \mathbf{IN}_r^* \mathbf{R}_r} - \frac{K_p + \mathbf{IER}}{K_{pr} + \mathbf{IER}_r} \right)^{-1} \quad (15)$$

$$B_2 = \left(\frac{K_{pr} + \mathbf{IN}_r^* \mathbf{R}_r}{\mathbf{IN}_r^* \mathbf{R}} - \frac{K_{pr} + \mathbf{I\,E\,R}}{K_p + \mathbf{I\,E\,R}} \right)^{-1} \quad (16)$$

These equations indicate that the stiffness tensor is independent of stress increments, and the stress and strain increments have a linear relationship. In these equations, if K_{pr} is set to be K_p and $\mathbf{R}_r$ to be $\mathbf{R}$, they

will be downgraded to the formulations in the classical plasticity.

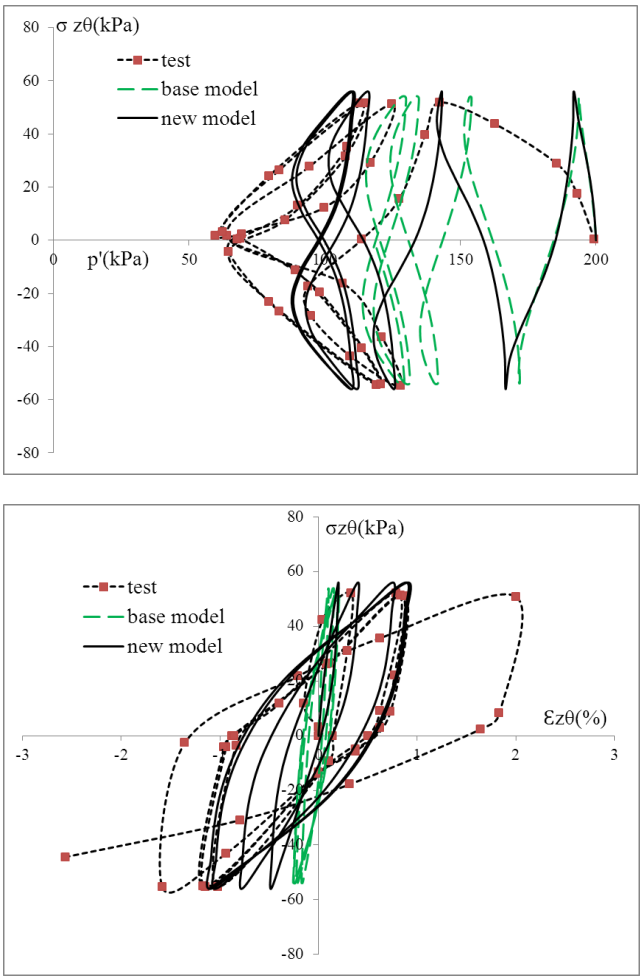

Figure 6. Test results and model predictions of the torsional shear tests in Chen & Kutter (2009)

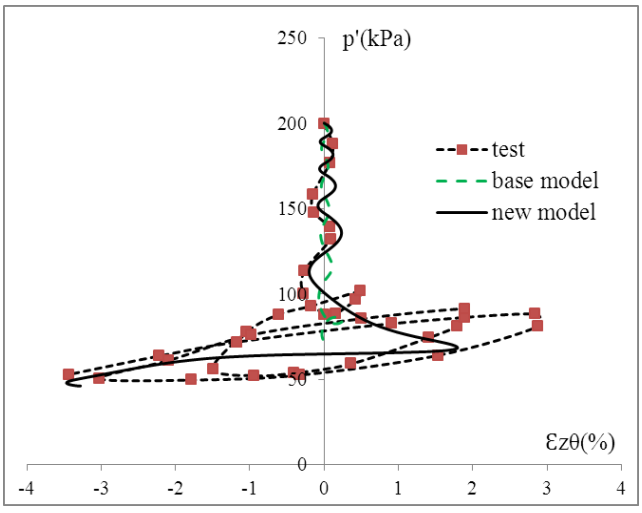

Figure 7. Test results and model predictions of the rotational shear tests in Chen & Kutter (2009)

Figures 2 and 3 show the drained predictions using the modified model for the tests in Miura et al (1986). These figures indicate that the new predictions have overall better agreements with the test results than the original predictions, especially for the shear and volumetric strains. Figures 6 and 7 show the new undrained predictions for Nevada sand, and they are able to reproduce the liquefaction, reflected by the large displacements.

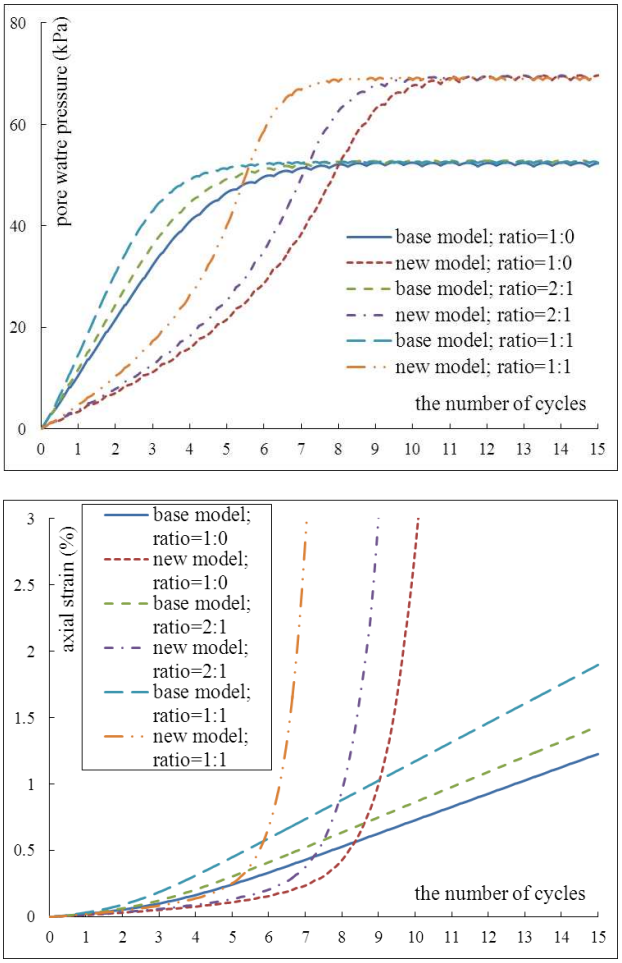

Figure 8. Predicted pore water pressure and axial strain with different ratios of shear amplitudes in two PSRs

The model performances with two PSRs along different directions are also studied. The tests by Miura et al (1986) are used as a reference. Its initial isotropic confining pressure is 98 kPa, and σ_x is increased to 196 kPa under the drained condition. The cyclic shear stresses τ_{xy} and τ_{xz} with different amplitudes are then applied under undrained conditions. τ_{xz} is one quarter of a cycle later than τ_{xy}. The amplitude of major shear τ_{xy} is always 10 kPa, and three cases of minor shear τ_{xz} are considered with their amplitudes of 0, 5 and 10 kPa, giving the ratio of shear amplitudes of 1:0, 2:1, 1:1, respectively. Figure 8 shows the predictions of pore water pressures and axial strains by using the modified and original model. There is not a sudden increase of strains in all these three loading cases, and therefore the liquefaction doesn't occur by using the original model. In contrast, the liquefaction takes place in all the cases by using the modified model. As discussed before, this is because the original model predicts a smaller plastic volumetric contraction (or even volumetric expansion) at a higher stress ratio for the PSR. Figure 8 also indicates that multiple PSRs make soil reach liquefaction faster than one PSR.

4 CONCLUSION

The paper first discusses the capability of a well-established kinematic hardening soil model in predicting stress-strain responses of soil under the PSR. It can predict the non-coaxiality very well, but its prediction of volumetric and shear strains is the poorest. The model is modified to independently treat the stress rate component generating the PSR. An additional flow rule and plastic modulus for the PSR stress rate are used, and the predictions are improved, especially for the shear strain component and volumetric strain. One important feature of the model is that it is developed in the general stress space with six stress variables, and it can take into account multiple PSRs. Another feature is that it retains the linear stress rate-strain rate relationship. Soil responses under multiple PSRs are also studied, and they can bring soil to failure faster than one PSR.

5 PREFERENCES

Chen, Y.R., Kutter, B.L. (2009), Contraction, dilation, and failure of sand in triaxial, torsional, and rotational shear tests, *Journal of engineering mechanics*, 135(10), 1155-1165

Dafalias, Y.F. & Manzari, M.T. (2004), Simple plasticity sand model accounting for fabric change effects, *Journal of Engineering Mechanics, ASCE*, 130(6), 622-634

Grabe, P.J. & Clayton, C.R.I. (2009), Effects of principal stress rotation on permanent deformation in rail track foundations, *Journal of Geotechnical and Geoenvironmental Engineering, ASCE*, 555-565

Gutierrez, M., Ishihara, K. & Towhata, I. (1991), Flow theory for sand during rotation of principal stress direction, *Soils and foundations*, 31(4), 121-132

Ishihara, K. & Towhata, I. (1983), Sand response to cyclic rotation of principal stress directions as induced by wave loads, *Soils and Foundations*, 23(4), 11-26

Ishihara, K. (1993), Liquefaction and flow failure during earthquakes, *Geotechnique*, 43(3), 351-415

Li, X.S. & Dafalias, Y.F. (2004), A constitutive framework for anisotropic sand including non-proportional loading, *Geotechnique*, 54(1), 41-55

Miura, K., Miura, S. & Toki, S. (1986), Deformation behavior of anisotropic dense sand under principal stress axes rotation, *Soils and Foundations*, 26(1), 36-52

Roscoe, K.H., Bassett, R.H. & Cole, E.R.L. (1967), Principal axes observed during simple shear of sand, *Proceedings of the Geotechnical Conference*, Oslo, 231-237

Tsutsumi, S. & Hashiguchi, K. (2005), General non-proportional loading behavior of soils, *International Journal of Plasticity*, 21, 1941-1969

Yang, Y. & Yu, H.S. (2006), A non-coaxial critical state model and its application to simple shear simulations, *International Journal for Numerical and Analytical Methods in Geomechanics*, 30, 1369-1390

Yang, Y. & Yu, H.S. (2012), A kinematic hardening soil model considering the principal stress rotation, *International Journal for Numerical and Analytical Methods in Geomechanics*, DOI:10.1002/nag.2138